A theoretical model for fibroblast-controlled growth of saccular cerebral aneurysms

Martin Kroon, Gerhard A. Holzapfel

www.elsevier.com/locate/yjtbi

A theoretical model for fibroblast-controlled growth of saccular cerebral aneurysms

Martin Kroon, Gerhard A. Holzapfel

PII: S0022-5193(08)00560-2
DOI: doi:10.1016/j.jtbi.2008.10.021
Reference: YJTBI 5344

To appear in: *Journal of Theoretical Biology*

Received date: 13 May 2008
Revised date: 3 October 2008
Accepted date: 25 October 2008

Cite this article as: Martin Kroon and Gerhard A. Holzapfel, A theoretical model for fibroblast-controlled growth of saccular cerebral aneurysms, *Journal of Theoretical Biology* (2008), doi:10.1016/j.jtbi.2008.10.021

A theoretical model for fibroblast-controlled growth of saccular cerebral aneurysms

Martin Kroon[a], Gerhard A. Holzapfel[a,b,*]

[a]*School of Engineering Sciences, Department of Solid Mechanics*
Royal Institute of Technology (KTH), 100 44 Stockholm, Sweden
[b]*Institute of Biomechanics, Graz University of Technology, 8010 Graz, Austria*

Submitted to *J. Theor. Biol.*; 3 November 2008

Abstract

A new theoretical model for the growth of saccular cerebral aneurysms is proposed by extending the recent constitutive framework of Kroon and Holzapfel (J. Theor. Biol., 247:775–787, 2007). The continuous turnover of collagen is taken to be the driving mechanism in aneurysmal growth. The collagen production rate depends on the magnitude of the cyclic deformation of fibroblasts, caused by the pulsating blood pressure during the cardiac cycle. The volume density of fibroblasts in the aneurysmal tissue is taken to be constant throughout the growth process. The growth model is assessed by considering the inflation of an axisymmetric membranous piece of aneurysmal tissue, with material characteristics representative of a cerebral aneurysm. The diastolic and systolic states of the aneurysm are computed, together with its load-free state. It turns out that the value of collagen pre-stretch, that determines growth speed and stability of the aneurysm, is of pivotal importance. The model is able to predict aneurysms with typical berry-like shapes observed clinically, and the predicted wall stresses correlate well with the experimentally obtained ultimate stresses of this type of tissue. The model predicts that aneurysms should fail when reaching a size of about 1.2-3.6 mm, which is smaller than what has been clinically observed. With some refinements, the model may, however, be used to predict future growth of diagnosed aneurysms.

Key words: Aneurysm; Saccular; Cerebral; Collagen; Membrane; Artery

1 Introduction

Rupture of an intracranial aneurysm and the resulting subarachnoid hemorrhage are serious events associated with high rates of mortality and morbidity. About 50% of patients die within one month after the event, and of those who survive more than one third have major neurologic deficits (Brisman et al., 2006; Schievink, 1997). Aneurysms are a common pathology only in human arteries and in some primates

* Corresponding author. Institute of Biomechanics, Center of Biomedical Engineering, Graz University of Technology, Kronesgasse 5-I, 8010 Graz, Austria. *E-mail address:* gh@biomech.tu-graz.ac.at (G.A. Holzapfel).

(Canham et al., 2006), and intracranial aneurysms are more prevalent in females than in males (Mettinger, 1982). Intracranial aneurysms usually do not rupture if they are less than 10 mm in diameter (Austin et al., 1993; Rinkel et al., 1998; Wiebers et al., 1981), and at clinical centres, cerebral aneurysms are considered as critical when their size is roughly larger than 5 mm. Considerable evidence supports the role of genetic factors in the pathogenesis of intracranial aneurysms (Schievink, 1997), but other factors, such as hemodynamic stress at arterial bifurcations, congenital medial defects, degenerative arterial wall changes, smooth muscle cell apoptosis, smoking and excessive alcohol consumption are also believed to contribute to aneurysmal development (Chen et al., 2004; Feigin et al., 2005; Matsubara et al., 2004; Pentimalli et al., 2004; Wermer et al., 2005). Once detected, the changes of the aneurysmal wall are already advanced or have been modified with other factors such as atherosclerosis (Kondo et al., 1998), and little is therefore known about the details of how they originate, grow, and rupture (Jamous et al., 2005). In order to shed some light upon the development process of cerebral aneurysms, a number of animal model aneurysms have been developed (AAssar et al., 2003; Espinosa et al., 1984; Hashimoto et al., 1984; Kamphorst et al., 1991; Kim and Cervos-Navarro, 1991; Kim et al., 1992; Kojima et al., 1986; Kondo et al., 1998; Miskolczi et al., 1998; Zhang et al., 2003). These models may give some guidance concerning the development process, but it remains unclear to what extent these models actually reflect the etiology of human aneurysms.

Cerebral arteries are muscular arteries having significantly less elastin in the media (than elastic arteries) and lacking the external elastic lamina. Most bifurcations of the cerebral vasculature are structurally stable, but a small number develop a weakness that causes the wall to expand outwardly in the region near the flow divider of the branching artery (Austin et al., 1993; MacDonald et al., 2000; Rowe et al., 2003). Some measurements of the macroscopic mechanical properties of cerebral arteries and aneurysms exist (Coulson et al., 2004; Monson et al., 2003, 2005; Scott et al., 1972; Steiger, 1990; Tóth et al., 1998, 2005) and the structural organisation of these tissues is fairly well documented (Canham et al., 1991b,a, 1992, 1996, 1999; Finlay et al., 1991, 1995, 1998; Hassler, 1972; MacDonald et al., 2000; Rowe et al., 2003; Smith et al., 1981; Whittaker et al., 1988). In the aneurysmal wall, the tunica media and the internal elastic lamina have often disappeared or are severely fragmented (Abruzzo et al., 1998; Sakaki et al., 1997; Stehbens, 1963; Suzuki and Ohara, 1978; Tóth et al., 1998). In either case, these layers do not seem to contribute significantly to the structural integrity of the aneurysmal wall. Thus, the wall of saccular cerebral aneurysms can roughly be described as a development of the adventitia of the original healthy artery (Abruzzo et al., 1998; Scanarini et al., 1978; Schievink, 1997). In the media of a healthy cerebral artery, the smooth muscle and collagen components are almost perfectly aligned in the circumferential direction of the artery (Finlay et al., 1995; Walmsley et al., 1983), whereas the collagen of the adventitia (which dominates the mechanical behaviour of this layer) shows a dispersion from the circumferential to the longitudinal orientation (Finlay et al., 1995; Smith et al., 1981).

The wall of an aneurysm is a living and metabolising structure, able to add to and reinforce itself. Enlargement does not necessarily imply thinning, because new collagen is added as the aneurysm expands. Collagen is a major component of blood vessels, and Type I and III collagen together represent about 80-90% of the total arterial collagen (Majamaa et al., 1992). The growth of aneurysms is associated with an increased collagen turnover (Mimata et al., 1997). Collagen is produced by fibre-producing cells such as fibroblasts and smooth muscle cells, and collagen degradation is accomplished by collagenases (Dobrin and Canfield, 1984; Murphy and Reynolds, 1985). Increased levels of collagenases have also been observed in aneurysmal tissue (AAssar et al., 2003; Anidjar et al., 1992; McMillan et al., 1995; Sluijter et al., 2004; Webster et al., 1991). The production of collagen (Type I) in cerebral aneurysms is mainly accomplished by fibroblasts (Eastwood et al., 1998; Espinosa et al., 1984; Kamphorst et al., 1991; Sluijter et al., 2004; Tóth et al., 1998), and these cells therefore play a key role in aneurysmal growth. Fibroblasts produce and organise the extracellular matrix (ECM). Conversely, the ECM influences the development, shape, migration, proliferation, survival, and function of the fibroblasts. The fibroblast belongs to the group of *adherent cells*, and attaches to the ECM by integrins (Cukierman et al., 2001; Jiang and Grinnell, 2005). The mobility of the fibroblast and its ability to contract the ECM are important properties in the maintenance of the ECM (Barocas et al., 1995; Dembo and Wang, 1999; Eastwood et al., 1998; Friedl and Bröcker, 2000; Friedrichs et al., 2007; Grinnell, 2003; Lo et al., 2000; Poole et al., 2005). The fibroblast also has the ability to align itself in the direction of existing collagen fibres and to produce new collagen that is aligned in the same direction (Birk et al., 1990; Cisneros et al., 2006; Friedrichs et al., 2007; Huang et al., 1993; Lin et al., 1999; Meshel et al., 2005; Tóth et al., 1998). Furthermore, the activity of adherent cells is strongly dependent upon mechanical stimuli from the surrounding ECM (Pelham and Wang, 1997; Weyts et al., 2003). More specifically, cyclic deformation (which fibroblasts embedded in an arterial wall are exposed to) is known to influence the proliferation and collagen production rate of fibroblasts (Butt et al., 1995; Eastwood et al., 1998; Lee et al., 2004; Wille et al., 2006; Wu and Chen, 2000), and both of these factors are important for the growth of aneurysmal tissue.

Several theoretical studies related to growth and remodelling of arterial tissue have been presented (e.g. Baek et al. (2006); Humphrey and Rajagopal (2002); Kroon and Holzapfel (2007a,b); Rachev et al. (1996); Ryan and Humphrey (1999); Taber and Humphrey (2001); Watton et al. (2004)). In the present paper, we propose a new theoretical model for the growth of human cerebral saccular aneurysms. The approach has a few similarities with a model previously proposed by Kroon and Holzapfel (2007a), but the present model has some important novelties. The model rests on the assumption that collagen is the only load-bearing constituent in the aneurysmal wall and that the continuous turnover of collagen is the driving mechanism for aneurysmal growth. The collagen is produced by fibroblasts, which are dispersed throughout the aneurysmal wall. The collagen production rate is taken to depend upon the number of fibroblasts available and the average production rate of

fibroblasts. The average production rate per fibroblast is, in turn, taken to depend on the cyclic deformation of the fibroblasts caused by the pulsating blood flow in the parent artery. An axisymmetric model is used to assess the new growth model.

In Section 2, we introduce the necessary continuum mechanics framework and give a detailed description of the model. To evaluate the proposed model, we use an axisymmetric membrane exposed to a surface pressure. The geometry, the finite element implementation, and the initial conditions of this numerical example is outlined in Section 3. In Section 4, we present some numerical results, which are further discussed and evaluated in the concluding Section 5.

2 A theoretical model for fibroblast-controlled growth and remodelling of thin aneurysmal tissue

The wall of a saccular cerebral aneurysm is modelled as a hyperelastic membrane, whose constitutive behaviour is governed by a 3D strain-energy function Ψ. We assume that collagen is the only load-bearing constituent in the aneurysmal wall, which is taken to be a development of the adventitia of the original healthy arterial wall. Remnants of media, internal elastic lamina, and intima may well still be present in the aneurysm, but are considered not to give any significant contribution to the mechanical strength of the aneurysmal wall. The continuous turnover of collagen is the driving mechanism for aneurysmal remodelling and growth. This remodelling and turnover of collagen is assumed to be accomplished by fibroblasts, which are spread throughout the collagen network.

2.1 Continuum mechanics framework

Consider the membrane in Fig. 1. We introduce a reference frame of right-handed, rectangular coordinate axes at a fixed origin with orthonormal basis vectors $\mathbf{e}_i$, $i = 1, 2, 3$. The position vector $\mathbf{X}$ in the reference configuration Ω_0 is given as

$$\mathbf{X} = X_i \mathbf{e}_i, \tag{1}$$

where X_i are the referential coordinates and are considered as being along the axes introduced. The position vector $\mathbf{x}$ in the current configuration Ω is

$$\mathbf{x} = x_i \mathbf{e}_i, \tag{2}$$

where x_i denote the related spatial coordinates. The same reference frame for the reference and current configurations was used.

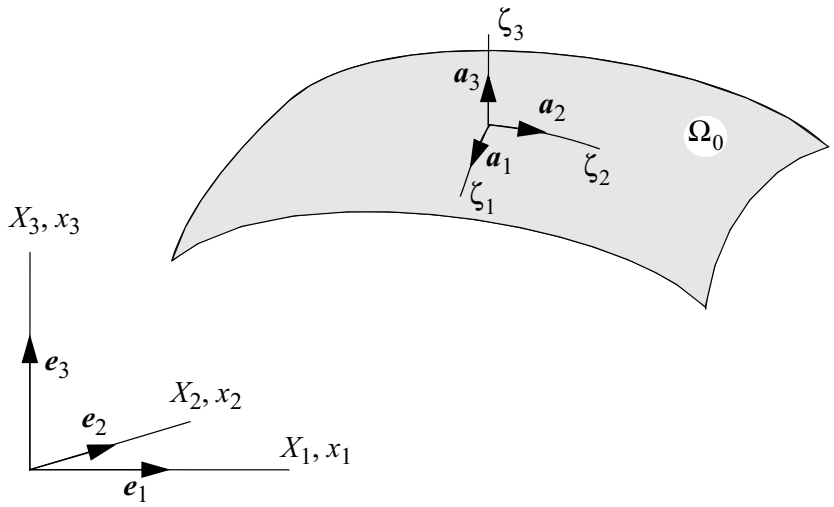

Fig. 1. The membrane in the reference configuration Ω_0 and its reference frame of rectangular coordinate axes at a fixed origin with orthonormal basis vectors $\mathbf{e}_i$, $i = 1, 2, 3$. The referential and the spatial coordinates are labelled as X_i and x_i, respectively, while ζ_1 and ζ_2 are the convected coordinates, and ζ_3 is a coordinate oriented normal to the membrane surface.

The displacement vector **u** is then defined as

$$\mathbf{u} = \mathbf{x} - \mathbf{X} = u_i \mathbf{e}_i. \tag{3}$$

Material points on the membrane are labeled by the surface convected coordinates ζ_1 and ζ_2, together with ζ_3 oriented normal to the membrane surface. Greek indices are used to denote the quantities measured by using the membrane intrinsic metric. The associated base vectors $\mathbf{a}_1$, $\mathbf{a}_2$ and $\mathbf{a}_3$ define a local Euclidean frame on the membrane, as indicated in Fig. 1. Derivatives with respect to the surface coordinates ζ_1, ζ_2 and ζ_3 in the reference configuration are denoted

$$(\bullet)_{,\alpha} = \frac{\partial(\bullet)}{\partial \zeta_\alpha}. \tag{4}$$

We define the deformation gradient **F** for this membrane according to

$$\mathbf{F} = \frac{\partial x_i}{\partial \zeta_\alpha} \mathbf{e}_i \otimes \mathbf{a}_\alpha. \tag{5}$$

The loading imposed on the aneurysm is caused by the blood pressure p in the parent artery. The pressure in a blood vessel varies in a pulsating manner, where the lowest pressure (at diastole) is denoted p_{dia} and the highest pressure (at systole) is denoted p_{sys}. We consider four different deformed configurations, see Fig. 2. Three of these configurations, Ω_{lf}, Ω_{dia} and Ω_{sys}, are associated with the applied pressure

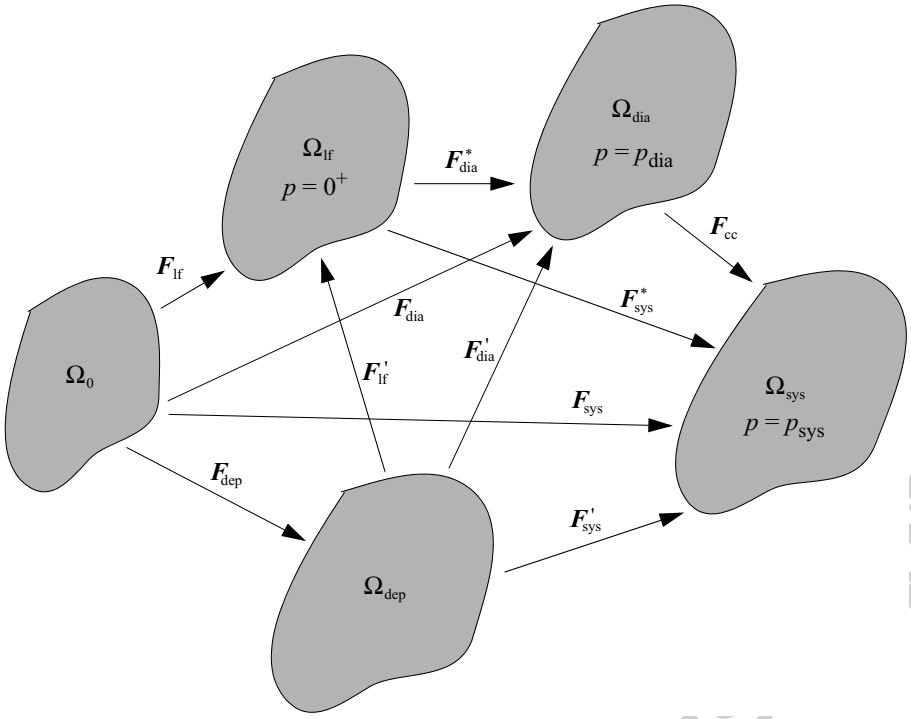

Fig. 2. Decomposition of the deformation gradient.

loads $p = 0^+$, $p = p_{\text{dia}}$ and $p = p_{\text{sys}}$, respectively. The configuration Ω_{lf} defines the load-free state of the aneurysm when an infinitesimally small pressure $p = 0^+$ is applied. (As will be evident later on, an applied pressure $p = 0$ would allow for an infinite number of possible deformation states, and therefore $p = 0^+$ is required in order to uniquely define the load-free state.) Due to the continuous remodelling of the collagen, the load-free configuration Ω_{lf} will, in general, not coincide with the reference configuration Ω_0. Since collagen fibres are continuously deposited as the aneurysm evolves and grows, fibres, deposited at different times, will have different natural configurations. In order to account for this, we also introduce a fourth deformed configuration, say Ω_{dep}, at which a specific fibre is deposited.

The total deformation gradient $\mathbf{F}$ is decomposed according to Fig. 2, where $\mathbf{F}$ is evaluated in the four deformed configurations Ω_{lf}, Ω_{dia}, Ω_{sys} and Ω_{dep}. We emphasise, that the deformation gradients in Fig. 2 do not signify mappings of whole configurations, but rather linear mappings of line elements within the configurations. The deformation gradients $\mathbf{F}_{\text{lf}}$, $\mathbf{F}_{\text{dia}}$ and $\mathbf{F}_{\text{sys}}$ describe the deformations from the reference configuration Ω_0 to the load-free (Ω_{lf}), the diastolic (Ω_{dia}) and the systolic (Ω_{sys}) states, respectively. The deformation gradients $\mathbf{F}^{\star}_{\text{dia}} = \mathbf{F}_{\text{dia}}\mathbf{F}^{-1}_{\text{lf}}$ and $\mathbf{F}^{\star}_{\text{sys}} = \mathbf{F}_{\text{sys}}\mathbf{F}^{-1}_{\text{lf}}$ denote the deformations experienced by the aneurysmal wall from the load-free configuration Ω_{lf} to the diastolic Ω_{dia} and systolic Ω_{sys} states, respectively. The entities $\mathbf{F}^{\star}_{\text{dia}}$ and $\mathbf{F}^{\star}_{\text{sys}}$ are introduced in order to quantify the *actual* deformation experienced by the aneurysmal wall at a certain point of time. The entity $\mathbf{F}_{\text{cc}} = \mathbf{F}_{\text{sys}}\mathbf{F}^{-1}_{\text{dia}}$ is the deformation from the diastolic state Ω_{dia} to the systolic state

$\Omega_{\rm sys}$, quantifying the cyclic deformation of the tissue during the cardiac cycle (the index 'cc' stands for 'cardiac cycle'). For all of the deformation gradients defined above, dependence on time t and $\mathbf{X}$ is understood.

The deformed configuration $\Omega_{\rm dep}$ is introduced in order to track the deformations of individual collagen fibres. The deformation gradient $\mathbf{F}_{\rm dep} = \mathbf{F}(t_{\rm dep})$ is the deformation at time $t_{\rm dep}$ at which a specific fibre is deposited. The deformations $\mathbf{F}'_{\rm lf} = \mathbf{F}_{\rm lf}\mathbf{F}_{\rm dep}^{-1}$, $\mathbf{F}'_{\rm dia} = \mathbf{F}_{\rm dia}\mathbf{F}_{\rm dep}^{-1}$ and $\mathbf{F}'_{\rm sys} = \mathbf{F}_{\rm sys}\mathbf{F}_{\rm dep}^{-1}$ quantify the subsequent deformation experienced by this particular fibre in the load-free, the diastolic and the systolic states, respectively. Thus, $\mathbf{F}'_{\rm lf}$, $\mathbf{F}'_{\rm dia}$ and $\mathbf{F}'_{\rm sys}$ will depend on t, $t_{\rm dep}$ and $\mathbf{X}$. The configurations $\Omega_{\rm lf}$, $\Omega_{\rm dia}$ and $\Omega_{\rm sys}$ will evolve with time t as the aneurysm grows, and at each time t a range of fibres with different natural configurations $\Omega_{\rm dep}$ will be active and contribute to the structural integrity of the aneurysmal wall.

The deformation gradient can be decomposed into a rotation $\mathbf{R}$ and a material stretch $\mathbf{U}$, according to $\mathbf{F} = \mathbf{R}\mathbf{U}$, and the associated right Cauchy-Green deformation tensor is then obtained as $\mathbf{C} = \mathbf{F}^{\rm T}\mathbf{F} = \mathbf{U}^2$ (Holzapfel, 2000). In general, the total deformation gradient $\mathbf{F}$ may be decomposed into $\mathbf{F} = \mathbf{F}_2\mathbf{F}_1$, where $\mathbf{F}_1 = \mathbf{R}_1\mathbf{U}_1$ and $\mathbf{F}_2 = \mathbf{R}_2\mathbf{U}_2$. However, we instead choose to express the total deformation gradient as $\mathbf{F} = \mathbf{R}_2\mathbf{U}_2\mathbf{U}_1$, i.e. as two material stretches $\mathbf{U}_1$ and $\mathbf{U}_2$ followed by a single rotation $\mathbf{R}_2$. Thus, the first deformation is taken to be a pure material stretch and all rotations of the total deformation are confined to the rotation $\mathbf{R}_2$. The following decompositions are now introduced:

$$\left.\begin{array}{lcl} \Omega_{\rm lf} & : & \mathbf{F}_{\rm lf} = \mathbf{R}_{\rm lf}\mathbf{U}_{\rm lf}, \\ \Omega_{\rm dia} & : & \mathbf{F}_{\rm dia} = \mathbf{R}_{\rm dia}\mathbf{U}_{\rm dia} = \mathbf{R}^{\star}_{\rm dia}\mathbf{U}^{\star}_{\rm dia}\mathbf{U}_{\rm lf}, \\ \Omega_{\rm sys} & : & \mathbf{F}_{\rm sys} = \mathbf{R}_{\rm sys}\mathbf{U}_{\rm sys} = \mathbf{R}^{\star}_{\rm sys}\mathbf{U}^{\star}_{\rm sys}\mathbf{U}_{\rm lf} = \mathbf{R}_{\rm cc}\mathbf{U}_{\rm cc}\mathbf{U}_{\rm dia}, \end{array}\right\} \tag{6}$$

and

$$\left.\begin{array}{lcl} \Omega_{\rm lf} & : & \mathbf{F}_{\rm lf} = \mathbf{R}'_{\rm lf}\mathbf{U}'_{\rm lf}\mathbf{U}_{\rm dep}, \\ \Omega_{\rm dia} & : & \mathbf{F}_{\rm dia} = \mathbf{R}'_{\rm dia}\mathbf{U}'_{\rm dia}\mathbf{U}_{\rm dep}, \\ \Omega_{\rm sys} & : & \mathbf{F}_{\rm sys} = \mathbf{R}'_{\rm sys}\mathbf{U}'_{\rm sys}\mathbf{U}_{\rm dep}. \end{array}\right\} \tag{7}$$

The associated decompositions of $\mathbf{C}$ are then

$$\left.\begin{array}{lcl} \Omega_{\rm lf} & : & \mathbf{C}_{\rm lf} = \mathbf{U}^2_{\rm lf}, \\ \Omega_{\rm dia} & : & \mathbf{C}_{\rm dia} = \mathbf{U}^2_{\rm dia} = \mathbf{U}_{\rm lf}\mathbf{C}^{\star}_{\rm dia}\mathbf{U}_{\rm lf}, \\ \Omega_{\rm sys} & : & \mathbf{C}_{\rm sys} = \mathbf{U}^2_{\rm sys} = \mathbf{U}_{\rm lf}\mathbf{C}^{\star}_{\rm sys}\mathbf{U}_{\rm lf} = \mathbf{U}_{\rm dia}\mathbf{C}_{\rm cc}\mathbf{U}_{\rm dia}, \end{array}\right\} \tag{8}$$

and

$$\left.\begin{array}{lcl} \Omega_{\rm lf} & : & \mathbf{C}_{\rm lf} = \mathbf{U}_{\rm dep}\mathbf{C}'_{\rm lf}\mathbf{U}_{\rm dep}, \\ \Omega_{\rm dia} & : & \mathbf{C}_{\rm dia} = \mathbf{U}_{\rm dep}\mathbf{C}'_{\rm dia}\mathbf{U}_{\rm dep}, \\ \Omega_{\rm sys} & : & \mathbf{C}_{\rm sys} = \mathbf{U}_{\rm dep}\mathbf{C}'_{\rm sys}\mathbf{U}_{\rm dep}, \end{array}\right\} \tag{9}$$

where the orthogonality property for the rotation tensor $\mathbf{R}$ and the symmetry of the material stretch tensor $\mathbf{U}$ have been used in addition to the property $\mathbf{C} = \mathbf{U}^2$. From the expressions above we can now compute $\mathbf{C}^{\star}_{\rm dia} = \mathbf{U}^{-1}_{\rm lf}\mathbf{C}_{\rm dia}\mathbf{U}^{-1}_{\rm lf}$, $\mathbf{C}^{\star}_{\rm sys} = \mathbf{U}^{-1}_{\rm lf}\mathbf{C}_{\rm sys}\mathbf{U}^{-1}_{\rm lf}$, $\mathbf{C}_{\rm cc} = \mathbf{U}^{-1}_{\rm dia}\mathbf{C}_{\rm sys}\mathbf{U}^{-1}_{\rm dia}$, $\mathbf{C}'_{\rm dia} = \mathbf{U}^{-1}_{\rm dep}\mathbf{C}_{\rm dia}\mathbf{U}^{-1}_{\rm dep}$, and $\mathbf{C}'_{\rm sys} = \mathbf{U}^{-1}_{\rm dep}\mathbf{C}_{\rm sys}\mathbf{U}^{-1}_{\rm dep}$. These entities will be actually used in the computations to follow. Thus, the type of decomposition used here (on the form $\mathbf{F} = \mathbf{R}_2\mathbf{U}_2\mathbf{U}_1$) allows us to express all needed deformation measures purely in terms of material stretches related to the reference configuration. Note that all material stretches are defined with respect to the local reference frame defined by the basis vectors $\mathbf{a}_i$, see Fig. 1.

2.2 Constitutive model

We now consider the structure of the aneurysmal tissue. The aneurysmal wall is assumed to consist of n discrete and distinct layers of collagen fibres (plies that form a laminate). Thus, from a mechanical point of view, the structural organisation and properties of the collagen completely determine the mechanical response of the aneurysmal wall. Within a layer (ply) with index i, the collagen fibres and the embedded fibroblasts are perfectly aligned in a direction ϕ_i, defined with respect to the local reference coordinate system, see Fig. 3. There is a continuously ongoing process of production and degradation of collagen within each layer, and this turnover is accomplished by the fibroblasts. Since the fibroblasts are oriented in the same direction ϕ_i as the collagen fibres, newly produced collagen is deposited in that direction as well, and the orientation of the fibres in the different layers is, therefore, preserved during the growth process.

The aneurysmal wall is assumed to have a constant total initial thickness H_0 in Ω_0 and each collagen layer is assigned an initial thickness of H_0/n. The fibre angles ϕ_i are defined according to

$$\phi_i = \frac{i-1}{n}\pi, \qquad 1 \leq i \leq n, \tag{10}$$

where the fibre orientations are thus uniformly distributed over the whole azimuthal range and $n \geq 2$ provides the even number of tissue layers.

Due to the pulsating blood pressure, the aneurysmal tissue – and thereby the embedded fibroblasts – is exposed to cyclic deformation, quantified by the entity $\mathbf{C}_{\rm cc} = \mathbf{U}^{-1}_{\rm dia}\mathbf{C}_{\rm sys}\mathbf{U}^{-1}_{\rm dia}$, according to $(8)_3$. The collagen production rate per fibroblast

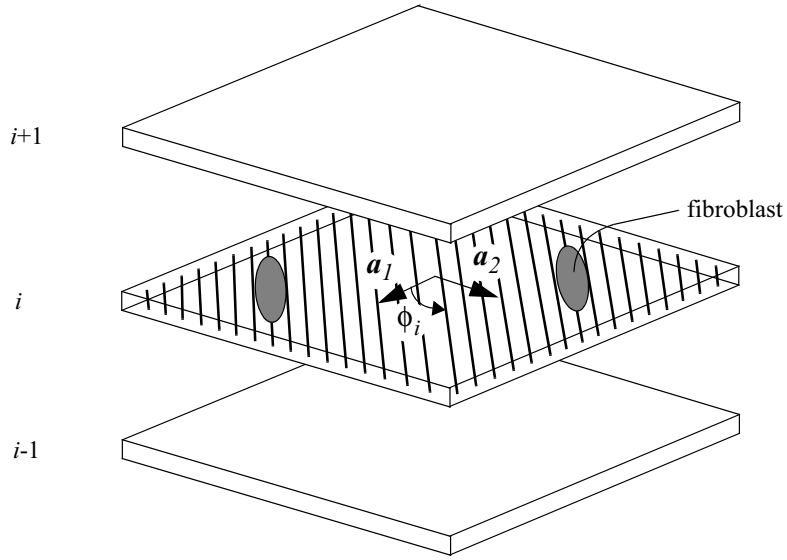

Fig. 3. The aneurysmal tissue is modelled as a multi-layered membrane consisting of n plies. Fibroblasts are embedded in the plies, and are aligned in the same direction as the fibres.

is assumed to be governed by the magnitude of the cyclic deformation of fibroblasts. In addition, fibroblasts are known to proliferate in growing tissue. We here assume that fibroblasts proliferate in order to maintain a constant fibroblast density in the growing tissue. The current number of fibroblasts per unit reference volume is denoted $n_{\rm fb}(t)$. This entity is taken to be constant through the tissue thickness and is expressed as

$$n_{\rm fb}(t) = n_{\rm fb\,0}\, J_{\rm lf}(t), \tag{11}$$

where $n_{\rm fb\,0} = n_{\rm fb}(t=0)$ is the concentration of fibroblasts in a healthy adventitia and $J_{\rm lf} = \det\mathbf{F}_{\rm lf}$. The mass production rate of collagen per unit reference volume in layer i, denoted $\dot{m}_i(t)$, is now expressed as

$$\dot{m}_i(t) = n_{\rm fb}(t)\beta_0 (C_{{\rm cc}\,i})^{\alpha}. \tag{12}$$

Thus, the collagen production rate $\dot{m}_i(t)$ depends on the current concentration of fibroblasts $n_{\rm fb}(t)$ and the cyclic deformation of these cells $C_{{\rm cc}\,i}$. The scalar $C_{{\rm cc}\,i}$ is defined as $C_{{\rm cc}\,i} = \mathbf{C}_{\rm cc} : \mathbf{A}(\phi_i)$, where $\mathbf{A}(\phi_i) = \mathbf{M} \otimes \mathbf{M}$ is a structure tensor, and $\mathbf{M}$ is a vector with components $M_1 = \cos\phi_i$, $M_2 = \sin\phi_i$, $M_3 = 0$ defining the direction of the fibres in layer i in the reference configuration. The influence of the scalar $C_{{\rm cc}\,i}$ on the collagen production rate is modulated by the exponent α. The parameter β_0 may roughly be interpreted as the mean collagen production rate per fibroblast of a healthy adventitia.

Fibroblasts continuously produce and degrade collagen fibres in the ECM. During production, collagen fibrils are deposited outside the fibroblast cell, and these fibrils are then inserted into the surrounding ECM. We assume that collagen fibrils, produced at time $t_{\rm dep}$, are inserted in the configuration $\Omega_{\rm sys}$, implying that $\mathbf{F}_{\rm dep} = \mathbf{F}_{\rm sys}(t_{\rm dep})$. However, fibroblasts also have the ability to contract the surrounding ECM, and the new collagen fibrils are, therefore, attached to the remaining ECM in a pre-stretched state. With regards to aneurysmal growth (and tissue remodelling in general), this pre-stretching is a very important mechanism and needs to be accounted for. It appears that the tractions imposed by the fibroblasts on the ECM are roughly proportional to the current stiffness of the ECM (Engler et al., 2004). Thus, we conjecture that collagen fibres, deposited at time $t_{\rm dep}$, are deposited in the configuration $\Omega_{\rm sys}$ with a constant pre-stretch $\lambda_{\rm pre}$. The total deformation $C_{\rm fib}$ of the fibres in the layer i, deposited at time $t_{\rm dep}$, can then be expressed as

$$C_{\rm fib} = \lambda_{\rm pre}^2 \mathbf{C}' : \mathbf{A}(\phi_i), \tag{13}$$

where $\mathbf{C}' = \mathbf{U}_{\rm dep}^{-1}(t_{\rm dep})\mathbf{C}(t)\mathbf{U}_{\rm dep}^{-1}(t_{\rm dep})$. The right Cauchy-Green tensors $\mathbf{C}$ and $\mathbf{C}'$ (defined with respect to Ω_0 and $\Omega_{\rm dep}$, respectively) are evaluated for the states $\Omega_{\rm lf}$ and $\Omega_{\rm dia}$, $\Omega_{\rm sys}$. Again, the entity $\mathbf{C}'$ will, in general, depend on the location $\mathbf{X}$, on current time t and on time of deposition $t_{\rm dep}$.

As a start, the strain energy $\psi_{\rm fib}$ per unit mass stored in the fibres is characterised by a simple polynomial, accounting for the highly nonlinear response of the wave-like collagen. Thus,

$$\psi_{\rm fib} = \mu(C_{\rm fib} - 1)^3, \quad C_{\rm fib} \geq 1, \tag{14}$$

where $\mu > 0$ is a positive material parameter, associated with the stiffness of collagen fibres. Note that Eq. (14) is valid when the fibres are in tension or are unloaded ($C_{\rm fib} \geq 1$), whereas the fibres are assumed to have zero stiffness in compression ($C_{\rm fib} < 1$).

The total strain energy $\Psi(t)$ per unit reference volume is then obtained by integration according to

$$\Psi(t) = \frac{1}{n}\sum_{i=1}^{n} \Psi_i(t) = \frac{1}{n}\sum_{i=1}^{n} \int_{-\infty}^{t} g(t, t_{\rm dep})\dot{m}_i(t, t_{\rm dep})\psi_{\rm fib}(t, t_{\rm dep}) {\rm d}t_{\rm dep}, \tag{15}$$

where $\Psi_i(t)$ is the strain energy of layer i, and g is the *life cycle function* (cf. Humphrey and Rajagopal, 2002; Kroon and Holzapfel, 2007a,b). This function g accounts for the turnover of the collagen fibres, and a simple pulse function is adopted according to

$$g(t, t_{\rm dep}) = \Theta(t - t_{\rm dep}) - \Theta(t - t_{\rm dep} - t_{\rm cl}), \tag{16}$$

where $\Theta(t)$ is the Heaviside step function, and t_{cl} is the life-time of the collagen fibres. This formulation implies that collagen fibres are assumed to have the same mechanical properties from the moment they are deposited to the end of their life time. Maturation and degradation of collagen fibres are taken to occur instantly at $t = t_{\mathrm{dep}}$ and $t = t_{\mathrm{dep}} + t_{\mathrm{cl}}$, respectively.

Membrane stresses are represented by a modified 2D second Piola-Kirchhoff stress tensor, with components defined as

$$S^{\star}_{\alpha\beta} = 2\frac{\partial \Psi}{\partial C^{\star}_{\alpha\beta}}, \tag{17}$$

with $\mathbf{C}^{\star} = \mathbf{U}_{\mathrm{lf}}^{-1}\mathbf{C}\mathbf{U}_{\mathrm{lf}}^{-1}$. The right Cauchy-Green tensors $\mathbf{C}$ and $\mathbf{C}^{\star}$ (defined with respect to Ω_0 and Ω_{lf}, respectively) are evaluated for the states Ω_{lf} and Ω_{dia}, Ω_{sys}. Since we consider a membrane, we only evaluate in-plane stresses, and α and β therefore only take on the values 1 and 2. This modified stress measure is employed in order to obtain physically relevant stresses. A modified corotated Cauchy stress $\sigma^{\star}_{\alpha\beta}$ is also defined as

$$\sigma^{\star}_{\alpha\beta} = \frac{H_0}{H_{\mathrm{lf}} J^{\star}} U^{\star}_{\alpha\gamma} S^{\star}_{\gamma\delta} U^{\star}_{\delta\beta}, \tag{18}$$

where $J^{\star} = \det \mathbf{U}^{\star}$, and H_{lf} is the current tissue thickness in the load-free state Ω_{lf}. In the deformation from Ω_{lf} to the diastolic and systolic states we assume incompressibility, which requires that $J^{\star} \equiv 1$. ($J^{\star}$ pertains to the fully 3D deformation of the tissue.) The tissue thickness will change as collagen is produced and degraded. By assuming that the volume density of collagen fibres in the load-free state Ω_{lf} is constant, H_{lf} can be estimated as

$$H_{\mathrm{lf}} = \frac{H_0}{n\lambda_1\lambda_2} \sum_{i=1}^{n} \frac{m_i}{m_0}. \tag{19}$$

where m_i and m_0 denote the current and initial collagen mass content, respectively, and λ_1 and λ_2 are the in-plane principal stretches in the load-free state Ω_{lf}. The determinant J_{lf} in Eq. (11) may then consequently be estimated as

$$J_{\mathrm{lf}} = \frac{H_{\mathrm{lf}}\lambda_1\lambda_2}{H_0} = \frac{1}{n}\sum_{i=1}^{n} \frac{m_i}{m_0}, \tag{20}$$

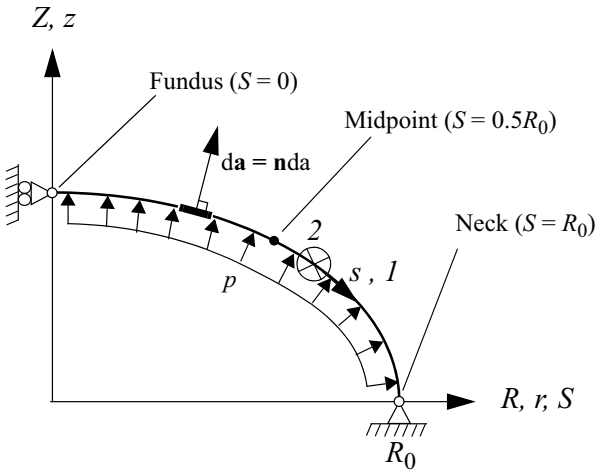

Fig. 4. Profile of the membrane, definitions of coordinates and principal directions, and loading and boundary conditions.

3 Numerical example: Inflation of an axisymmetric membrane

3.1 FE formulation for an axisymmetric membrane

A saccular cerebral aneurysm is here modelled as an axisymmetric membrane, which is hinged along its periphery and exposed to a (blood) pressure p. The membrane formulation used here is based on a work by Fried (1982) (also utilised by Kroon and Holzapfel (2007a) and Kyriacou et al. (1996)), and a brief review of the formulation is provided below.

Consider the axisymmetric membrane, as illustrated in Fig. 4. The surface profile can be parameterised using coordinates S and s in the reference and current configurations, respectively. Coordinates $R(S)$, $Z(S)$, $r(s)$, and $z(s)$ denote cylindrical coordinates in the reference and current configurations, respectively. The membrane is hinged at $R = R_0$. Boundary conditions are thus imposed according to

$$\left.\begin{array}{lcl} R = 0 & : & r = 0, \\ R = R_0 & : & r = R_0 \quad \text{and} \quad z = 0, \end{array}\right\} \tag{21}$$

see Fig. 4.

Principal directions 1 and 2 coincide with the direction of s and the circumferential direction, respectively, as indicated in Fig. 4. The convected surface coordinates ζ_1 and ζ_2, introduced in the previous section, are taken to coincide with the principal directions 1 and 2 in Fig. 4, respectively. The principal stretches in the plane of the

membrane can be expressed as

$$\lambda_1 = \frac{\mathrm{d}s}{\mathrm{d}S} = \sqrt{\left(\frac{\mathrm{d}r}{\mathrm{d}S}\right)^2 + \left(\frac{\mathrm{d}z}{\mathrm{d}S}\right)^2}, \quad \lambda_2 = \frac{2\pi r}{2\pi R} = \frac{r}{R}. \tag{22}$$

The potential energy Π of the membrane, inflated by a given constant pressure p is

$$\Pi = \int_{\Omega_0} \Psi \mathrm{d}V - p \int_{\partial\Omega_\sigma} \mathbf{u} \cdot \mathrm{d}\mathbf{a} = \pi \int_0^{R_0} \left(2R \sum_{i=1}^{n} \frac{H_0}{n} \Psi_i - pr^2 \frac{\mathrm{d}z}{\mathrm{d}S}\right) \mathrm{d}S, \tag{23}$$

where Ψ is the total strain energy per unit volume of the membrane, Ω_0 is the reference region of the membrane, with the infinitesimal volume element $\mathrm{d}V$ defined in that region, and $\partial\Omega_\sigma \subset \partial\Omega$ is the current boundary surface on which the pressure boundary condition acts. The second term in Eq. (23) denotes the energy contribution due to the pressure p. In that term $\mathrm{d}\mathbf{a} = \mathrm{d}a\mathbf{n}$ is a vector element of an infinitesimally small area defined in the current configuration, where $\mathbf{n}$ is the direction of the (pointwise) outward unit vector, which is perpendicular to the pressure loaded surface $\partial\Omega_\sigma$ of the membrane region, and $\mathrm{d}a$ is an infinitesimal surface element in the current configuration (see Fig. 4). The displacement vector is denoted by $\mathbf{u}$. Making use of the symmetry conditions, the volume integrals can be recast into a one-dimensional form, as indicated in Eq. $(23)_2$.

Equation $(23)_2$ is solved by using the finite element method with quadratic line elements. The membrane is discretised in the S direction by nodes distributed with a constant distance h in the reference configuration. The current geometry for an element is approximated according to

$$r(\xi) = \frac{1}{2}\xi(\xi - 1)r_1 + (1 - \xi^2)r_2 + \frac{1}{2}\xi(\xi + 1)r_3, \tag{24}$$

where $\xi \in [-1, 1]$, and r_1, r_2 and r_3 are the nodal values of r. In a similar way R and z are approximated. According to Eq. $(23)_2$, the potential energy Π_e for an element can thus be expressed as

$$\Pi_\mathrm{e} = \pi \int_{-1}^{1} (2R \sum_{i=1}^{n} \frac{H_0}{n} \Psi_i - pr^2 z' \frac{1}{h}) h \mathrm{d}\xi, \tag{25}$$

where $(\bullet)'$ denotes differentiation with respect to ξ. Since S can be written as, e.g., $S = S_0 + h\xi$, it follows that $\mathrm{d}S = h\mathrm{d}\xi$. The integration in Eq. (25) is approximated using Gauss integration, i.e.

$$\Pi_\mathrm{e} \approx \pi h \sum_{j=1}^{2} \left[2R(\xi^j) \sum_{i=1}^{n} \frac{H_0}{n} \Psi_i(\xi^j) - pr^2(\xi^j) z'(\xi^j) \frac{1}{h}\right], \tag{26}$$

where ξ^1, ξ^2 denote the coordinates for the Gauss points, and the related weights are 1. The approximated total potential energy is achieved by a summation over all elements. Nodal values for r and z are stored in a vector $\mathbf{q} = (r_1, \ldots, r_{n_n}\ z_1, \ldots, z_{n_n})^{\mathrm{T}}$, where n_n is the number of nodes in the model. To find the equilibrium state, the potential energy Π is minimised with respect to $\mathbf{q}$ using a Newton-Raphson scheme.

3.2 Initial conditions

Initial conditions are required for the strain-energy function. In a healthy artery, the load is mainly carried by the media, but as the media is degraded in a developing aneurysm, the load from the blood pressure is transferred to the adventitia. The initial conditions used here correspond to an instant transfer of the load from the media to the adventitia. Thus, in the half-closed time interval $t \in (-\infty, 0]$, the membrane is taken to have existed in the reference configuration with a surface pressure $p = 0$, with the collagen production rate $\dot{m}_i$ and the deformation C_{fib} in the fibres according to

$$\begin{aligned} \dot{m}_i(t \leq 0) &= n_{\mathrm{fb}\,0}\,\beta_0[\mathbf{I} : \mathbf{A}(\phi_i)]^{\alpha} = n_{\mathrm{fb}\,0}\,\beta_0, \\ C_{\mathrm{fib}}(t \leq 0) &= \lambda_{\mathrm{pre}}^2 \mathbf{I} : \mathbf{A}(\phi_i) = \lambda_{\mathrm{pre}}^2, \end{aligned} \tag{27}$$

respectively, where $\mathbf{I}$ is the unit tensor. Accordingly, using Eqs. (14) and (27) in Eq. (15), the strain energy per unit reference volume is for $t \leq 0$

$$\Psi(t \leq 0) = \frac{1}{n} \sum_{i=1}^{n} \int_{t-t_{\mathrm{cl}}}^{t} n_{\mathrm{fb}\,0}\,\beta_0 \mu (\lambda_{\mathrm{pre}}^2 - 1)^3 \mathrm{d}t_{\mathrm{dep}} = n_{\mathrm{fb}\,0}\,\beta_0 \mu (\lambda_{\mathrm{pre}}^2 - 1)^3 t_{\mathrm{cl}}. \tag{28}$$

3.3 Computation of the load-free state Ω_{lf}

From time $t = 0^+$ and onwards, the membrane is exposed to a pressure load that pulsates between p_{dia} and p_{sys}, and the development of the aneurysm is initialised. The time-dependent aneurysmal growth process is discretised using a constant time increment Δt. It is emphasised, that the analysis is completely quasi-static, and we are not modelling the fully dynamic deformation that a real aneurysm undergoes during the cardiac cycle. Thus, at each time step, we compute the deformed states Ω_{dia} and Ω_{sys} for the applied loads p_{dia} and p_{sys}, respectively, and these states are used to predict the growth of the aneurysm, as described in the growth model presentation above. In addition, we need the load-free state Ω_{lf}. However, finding Ω_{lf} is not a trivial task. The collagen fibres are assumed to have zero stiffness in compression, which means that by trying to find the solution for $p = 0^+$ we are approaching

deformation states in which the material has zero stiffness. From a numerical point of view this is somewhat tricky.

Hence, we proceed as follows: when estimating the load-free state $\Omega_{\rm lf}$ we first apply a pressure of $0.2\,p_{\rm dia}$ and compute the related deformed state $\Omega_{0.2}$. Hence, the nodal displacement vector $\mathbf{q} = (r_1, \ldots, r_{n_n} \;\; z_1, \ldots, z_{n_n})^{\rm T}$ is known for the three deformed states $\Omega_{0.2}$, $\Omega_{\rm dia}$ and $\Omega_{\rm sys}$. Second, the nodal positions in the state $\Omega_{\rm lf}$ are established by an extrapolation from the nodal positions in the states $\Omega_{0.2}$, $\Omega_{\rm dia}$ and $\Omega_{\rm sys}$. Thus, for a node with index i, six points are defined according to $(0.2p_{\rm dia}, r_{i,0.2})$, $(p_{\rm dia}, r_{i,\rm dia})$, $(p_{\rm sys}, r_{i,\rm sys})$, $(0.2p_{\rm dia}, z_{i,0.2})$, $(p_{\rm dia}, z_{i,\rm dia})$, and $(p_{\rm sys}, z_{i,\rm sys})$, denoting nodal displacements at the three different pressure levels considered. For the radial displacements, a curve of the form $r = a_1 + a_2 \exp(a_3 p)$ is fitted to the three points $(0.2p_{\rm dia}, r_{i,0.2})$, $(p_{\rm dia}, r_{i,\rm dia})$, $(p_{\rm sys}, r_{i,\rm sys})$. When the fitting parameters a_1, a_2 and a_3 have been determined, the radial displacement for the load-free state, $r_{i,0}$, can be estimated by evaluating the fitted curve for $p = 0$. In a similar way, another function on the same form is fitted to the points $(0.2p_{\rm dia}, z_{i,0.2})$, $(p_{\rm dia}, z_{i,\rm dia})$, $(p_{\rm sys}, z_{i,\rm sys})$, and the vertical displacement for the load-free state, $z_{i,0}$, can then be estimated by again evaluating the fitted curve for $p = 0$. This procedure is repeated for all nodal displacements at all time steps.

4 Numerical results

4.1 Geometrical and physical parameters

The aneurysmal growth model includes a number of geometrical and physical entities that need to be specified. The systolic blood pressure in a human carotid artery is about 7.0 kPa (Chatziprodromou et al., 2007), and this pressure is taken to apply for a cerebral artery in the vasculature of the Circle of Willis. Assuming a ratio of 120/80 between the systolic and diastolic blood pressures under healthy conditions, gives the respective pressure levels of $p_{\rm sys} = 7.0\,$kPa and $p_{\rm dia} = 4.7\,$kPa. The radius of a middle cerebral artery is about 1.2 mm, which gives the estimation $R_0 = 1.2\,$mm (Monson et al., 2005), and the thickness of a healthy adventitia is about $H_0 = 30\mu$m (Smith et al., 1981). The stiffness of the collagen fabric of the adventitia is accounted for by the factor $n_{\rm fb\,0}\,\beta_0 \mu t_{\rm cl} = 3.3\,$MPa (Monson et al., 2005). In the collagen production law (Eq. (12)), the exponent may be estimated to $\alpha = 3.0$ (Lee et al., 2004). There are two parameters that are difficult to estimate, namely the life-time $t_{\rm cl}$ of the collagen fibres and the pre-stretch $\lambda_{\rm pre}$ of collagen fibres. The collagen life-time sets the time-scale for the aneurysmal growth process and may be found in the range of 6 to 180 days (Humphrey, 1999). Aneurysmal tissue is known to exhibit a higher rate of collagen turnover than healthy tissue (Abdul-Hussien et al., 2007). The collagen pre-stretch $\lambda_{\rm pre}$ is very important for the mechanical behaviour of the aneurysmal wall, and in the following numerical investigation a particular emphasis is therefore put on the influence of this parame-

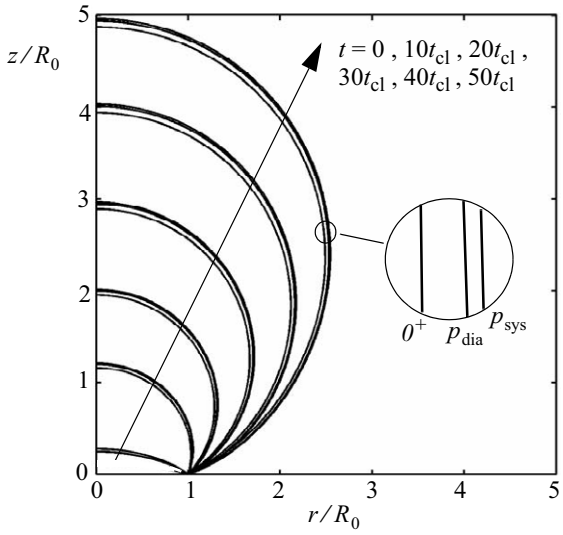

Fig. 5. Evolution of load-free, diastolic and systolic states of the aneurysm with time ranging from $t = 0$ to $t = 50t_{\mathrm{cl}}$ ($\lambda_{\mathrm{pre}} = 1.028$).

ter on the overall mechanical response. In the following numerical study, the time scale is normalised by the collagen life-time t_{cl}, and the time increment used in the computations was $\Delta t = 0.01t_{\mathrm{cl}}$.

4.2 Numerical analysis of aneurysmal growth

We start to explore some of the general features of the proposed growth model. Figure 5 shows how the aneurysm evolves with time for a case with $\lambda_{\mathrm{pre}} = 1.028$. The geometry of the aneurysm is normalised with the initial radius R_0, and the aneurysm is shown at six different stages of development. At each stage, the three configurations Ω_{lf}, Ω_{dia}, Ω_{sys} are shown. The size of the aneurysm increases approximately linearly with time, and after a time of $50t_{\mathrm{cl}}$ it has reached a size of about $5R_0$ (both in terms of height and maximum diameter). This corresponds to a size of 6 mm ($R_0 = 1.2$ mm). Since the life-time of collagen fibres is about 6-180 days, the time $50t_{\mathrm{cl}}$ thus corresponds to 300 days to about 25 years. At all time stages in Fig. 5, the diastolic and systolic states are quite close to each other, whereas the load-free states are more easily distinguishable.

The aneurysmal growth model depends strongly on the parameter λ_{pre}. Figure 6 shows how the size of the aneurysm evolves with time for different values of λ_{pre}. The size of the aneurysm is quantified in terms of the displacement of the fundus in the z-direction at systole. For $\lambda_{\mathrm{pre}} = 1.028$, the aneurysm grows with an approximately constant speed. For values of λ_{pre} lower than this, the growth speed increases in an accelerating manner, whereas for values of λ_{pre} higher than 1.028, the size of the aneurysm reaches a peak and then starts shrinking. This type of shrink-

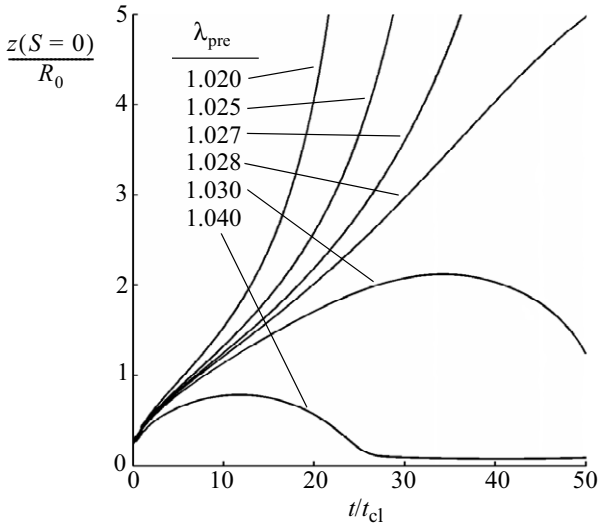

Fig. 6. Evolution of the aneurysm size (displacement of the fundus in the z-direction at systole normalised by R_0) for different values of λ_{pre}.

ing appears when the contractile 'force' caused by the pre-stretching of fibres is stronger than the applied blood pressure. Conversely, for values of λ_{pre} lower than 1.028, this contractile force is too weak to prevent accelerating aneurysm growth.

Figures 7(a) and (b) show the growth speed $\dot{z}$ of the fundus in the z-direction at systole in some more detail. The growth speed is normalised by the entity R_0/t_{cl}. Figure 7(a) shows the growth speed as a function of time, and Fig. 7(b) shows it as a function of aneurysm size. As noted previously, the growth speed for $\lambda_{\mathrm{pre}} = 1.028$ is fairly constant, whereas for values of λ_{pre} lower or higher than this leads to accelerating or decelerating growth, respectively. Initially, there is a pronounced peak in the growth speeds in both Figs 7(a) and (b). This peak appears as the aneurysm passes from a resting reference state ($t \leq 0$), with no blood pressure applied, to a mode where it pulsates between the diastolic and systolic states ($t > 0$). This instant application of the blood pressure is convenient for the present analysis but somewhat artificial, as are the initial growth speeds.

Initially, the aneurysm (or adventitia) has a uniform thickness H_0, but due to the addition of new material, the thickness distribution will change and become inhomogeneous. This phenomenon is illustrated in Fig. 8, where the ratio H_{lf}/H_0 is displayed as a function of the curvilinear coordinate S (normalised by R_0) for the case with $\lambda_{\mathrm{pre}} = 1.028$. Note that S/R_0 is zero at the fundus of the aneurysm and unity at the neck. Figure 8 shows the distribution of H_{lf}/H_0 at six different times. For $t = 0$, no net growth has yet occurred, and the ratio equals unity. The thickness of the aneurysm increases monotonically with time up to $t = 50t_{\mathrm{cl}}$, and by then it has reached a maximum ratio of almost $H_{\mathrm{lf}}/H_0 = 9$, implying that $H_{\mathrm{lf}} = 270\mu$m. After a time of about $20t_{\mathrm{cl}}$, a peak in the thickness distribution may be observed. During the subsequent development of the aneurysm, this peak becomes more and

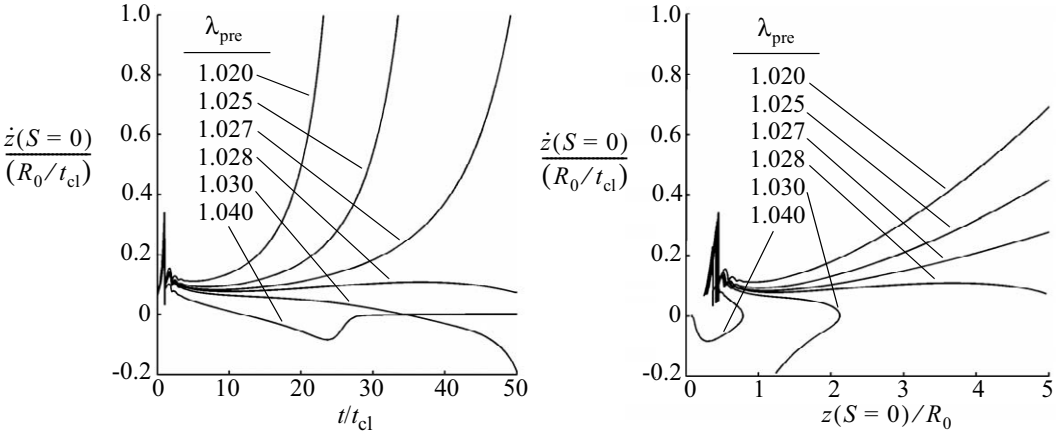

Fig. 7. Speed of the fundus in the z-direction at systole normalised by R_0/t_{cl} as a function of (a) time and (b) size. Solutions for different values of λ_{pre} are shown.

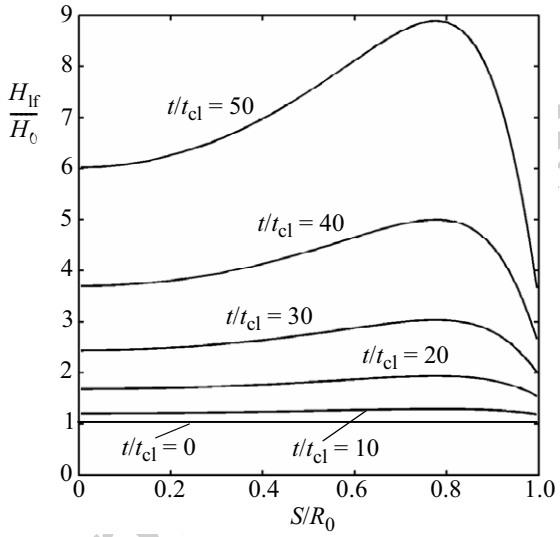

Fig. 8. Evolution of the normalised thickness distribution ($\lambda_{\mathrm{pre}} = 1.028$).

more pronounced. At $t = 50t_{\mathrm{cl}}$, there is a distinct thickness peak located at approximately $S = 0.8R_0$. The thickness increase is actually lowest at the neck of the aneurysm. The ratio between the highest and lowest thickness at $t = 50t_{\mathrm{cl}}$ is about 2.5.

Another field parameter of interest is the true (Cauchy) stress of the aneurysmal wall. For the present growth model, the maximum principal stress is always oriented in the principal direction 1. Figure 9 shows the evolution of the distribution of the maximum principal stress $\sigma_1^\star$ (at systole), computed on the basis of the modified Cauchy stress, as introduced in Eq. (18) ($\lambda_{\mathrm{pre}} = 1.028$). The stress is presented in absolute numbers. Initially, the stress is rather evenly distributed over the aneurysmal surface and reaches a value slightly below 0.5 MPa. As the aneurysm

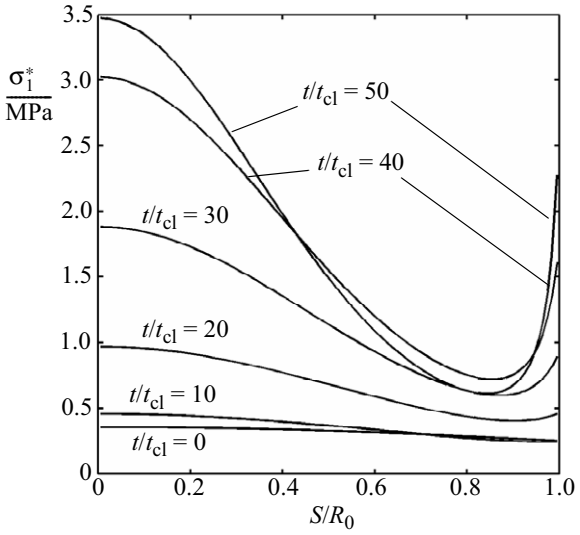

Fig. 9. Evolution of the maximum principal stress $\sigma_1^\star$ based on the modified stress measure in Eq. (18) ($\lambda_{\mathrm{pre}} = 1.028$).

evolves, the stresses increase monotonically. At all times, the peak stress appears at the fundus. At $t = 50t_{\mathrm{lf}}$, the peak stress is almost 3.5 MPa. However, the stress at the neck also reaches notable levels. The high stresses at the neck may, though, to some extent be caused by the rigid boundary condition imposed there. In a real aneurysm, that is situated in a more compliant environment, the stress concentration at the neck may not be as pronounced as here. The aneurysmal model also predicts that the stresses over the aneurysmal surface may differ significantly. For the most advanced state in Fig. 9 ($t = 50t_{\mathrm{lf}}$), the ratio between the highest stress (at the fundus) and lowest stress (at $S = 0.84R_0$) is about 5.6. The location of the lowest stress roughly coincides with the peak in the thickness distribution in Fig. 8.

Figs 10(a) and (b) show some additional aspects of the maximum principal stress. In Fig. 10(a), the stress distributions for the solutions of different values of λ_{pre} are compared at a specific aneurysm size ($z(S = 0) = 2R_0$) at systole. Thus, at a certain aneurysm size, a lower value of λ_{pre} tends to cause a higher level of stress in the aneurysmal wall. Since we are considering a membrane exposed to a surface pressure, the Cauchy stresses in the aneurysmal wall are determined by the principal curvatures of the membrane together with the current thickness of the membrane. A lower value of λ_{pre} renders the aneurysmal wall more compliant. Thus, for a given aneurysm size at systole, a more compliant aneurysmal wall will have undergone larger deformations and thereby experienced a higher degree of thinning (due to material incompressibility). This is probably the main reason why lower values of λ_{pre} result in higher stresses for a given aneurysm size at systole.

In Fig. 10(b), the peak stress at the fundus $\sigma_1^\star(S = 0)$ is plotted versus the aneurysm size at systole. Again, solutions for different values of λ_{pre} are included. The ulti-

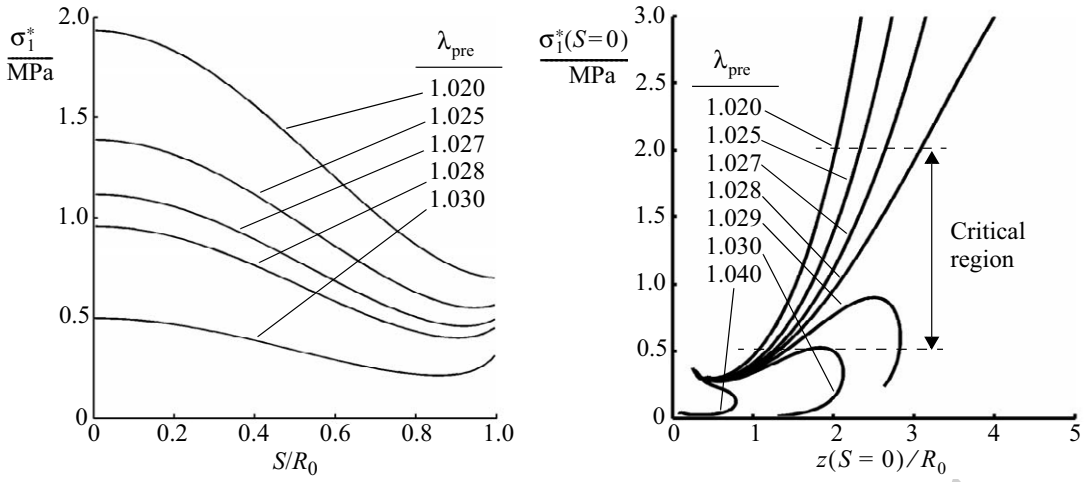

Fig. 10. (a) Distributions of the maximum principal stress $\sigma_1^\star$ for solutions of different values of $\lambda_{\rm pre}$ but at a fixed aneurysm size $z(S=0)=2R_0$; (b) fundus stress $\sigma_1^\star(S=0)$ versus aneurysm size at systole normalised by R_0 for different values of $\lambda_{\rm pre}$. Critical stress range, obtained from experiments, is indicated.

mate stress of cerebral aneurysmal tissues have been obtained experimentally and falls in a range of about 0.5-$2.0\,$MPa (Humphrey, 2002; MacDonald et al., 2000). This critical range is also indicated in Fig. 10(b). For the values of $\lambda_{\rm pre}$ considered in the present study, the critical aneurysm size at which rupture may be most frequently expected is between R_0 and $3R_0$. For our choice $R_0 = 1.2\,$mm, this translates to a size of 1.2 to 3.6 mm in absolute numbers.

5 Discussion and concluding remarks

In the present paper, we have proposed a new theoretical model for the growth of saccular cerebral aneurysms. More specifically, we have considered an axisymmetric membranous piece of tissue, exposed to a surface pressure, and with material characteristics representative for cerebral aneurysms. The new model is based upon a previously presented model (Kroon and Holzapfel, 2007a,b), but there are some important differences between them. In the previous model, we only considered two deformed states, i.e. the state where fibres were deposited and the systolic state. In the new model, however, we also introduce the diastolic state and the load-free state. A key feature of the new model is that the collagen production rate of the fibroblasts is governed by the cyclic deformation imposed on these cells during the cardiac cycle, i.e. the cyclic deformation between the diastolic and systolic states.

It is a well established fact that biological cells respond to mechanical stimuli, however, it is not clear whether cell reaction is triggered by mechanical *stress* or mechanical *deformation/strain* (see Humphrey (2001) for a nice discussion on this

topic). Correlating cell response with, say, the Cauchy stress (cf., for example, Baek et al. (2006)) has the advantage that only knowledge of the current deformed state (together with loads and boundary conditions) is required. On the other hand, the use of a strain (deformation) measure requires knowledge of *two* states, since strain is, by definition, defined as the deformation change between two states. Normally, strain is defined as the deformation change between a reference state and the current deformed state. However, for growing soft biological tissues, a reference configuration can, in general, not be defined in a meaningful way since the load-free configuration is continuously updated. However, in the present paper, we use the deformation between the diastolic and systolic states and correlate cell (fibroblast) response with the magnitude of this cyclic deformation. Thus, the present paper is an important contribution to the ongoing discussion of the mechanical sensing of cells since we show that a well-defined deformation measure – a measure that is in principle obtainable without knowledge of any reference configuration – can indeed be obtained and correlated with mechanical sensing and resulting activity of biological cells.

In the present study, we use membrane theory to model the aneurysm wall. The applicability of membrane theory is determined by the ratio of the wall thickness over the radius of the aneurysm. Initially, this ratio is $30\,\mu\text{m}/1.2\,\text{mm} = 0.025$, which means that the use of membrane theory is reasonably justified. For the numerical example that we show, this ratio has increased to 0.045 at the end of the analysis. Thus, due to the (finite) wall thickness of cerebral aneurysm walls, bending stresses will be present, however, they will probably be very small in comparison to (normal) membrane stresses.

The model includes a number of parameters. Most of these can be estimated fairly well on the basis of experimental surveys. Two parameters, however, are difficult to obtain (from the literature), namely the collagen life-time t_{cl} and the pre-stretch λ_{pre} of the collagen fibres. The collagen life-time essentially sets the time-scale of the aneurysmal growth process. The collagen pre-stretch λ_{pre} determines both the growth speed of the aneurysm and its stability properties. Hence, the collagen pre-stretch is of pivotal importance within the growth process. A numerical study was performed, and the results indicate that λ_{pre} should be roughly of the order 1.02-1.04. For lower values in this range, the growth process would continue at an accelerating speed, and for higher values, the process would decelerate and even cause the aneurysm to shrink back to a configuration close to its original reference state. This may actually be interpreted as a recovery of the arterial wall.

In experimental studies, single fibroblasts have been placed on 2D collagen gels, and fibroblasts have then been observed to contract the collagen gel with up to 15-20% (Engler et al., 2004). This would enable a pre-stretching of collagen fibres considerably higher than the pre-stretches used in the present study. However, this experimental result was for a 2D surface, which is easier to contract than a 3D matrix (provided that the stiffness of the material is the same). In addition, the max-

imum contraction that the fibroblast is able to impose on the ECM only serves as an upper limit to the pre-stretching of collagen fibres, and the actual pre-stretching by which fibres are attached may well be lower than this number.

In the predicted stress distributions over the aneurysmal surface, the peak stress always appears at the fundus, which makes sense since real aneurysms tend to rupture at this location (Canham et al., 2006). The ultimate stress of tissues from cerebral aneurysms have been experimentally obtained, and this fact allowed us to predict the size range for which the aneurysm could be expected to fail, see Fig. 10(b). It was predicted that aneurysms should fail approximately in the size range 1.2 to 3.6 mm. However, aneurysms usually do not rupture when smaller than 10 mm in size (Austin et al., 1993; Rinkel et al., 1998; Wiebers et al., 1981). Hence, the predicted range is below what has been observed clinically. As discussed earlier, the Cauchy stresses in the aneurysmal wall are determined by the principal curvatures of the membrane together with the current thickness. One reason why the stresses are overestimated in the model could be that the thickness of the aneurysmal wall is underestimated by the model. Another reason could be that the shape of the aneurysm is somewhat misrepresented by the axisymmetric model used here, leading to inaccurate surface curvature predictions.

Even though the size of the aneurysm is currently used as an indicator to determine the risk of rupture, it has been suggested that the growth *rate* of the aneurysm may also be a strong indicator of the rupture risk (Imaizumi et al., 2002; Kamitani et al., 1999). The growth rate of the present model aneurysm depends strongly on the life-time of the collagen fibres. In principle, the collagen life-time t_{cl} could be estimated if accurate growth rate data from clinical studies on aneurysms were available. Such data do in fact exist, but the scatter in these growth rate data is enormous. Yamaki et al. (1986), for example, report about a cerebral aneurysm that enlarged from 2 mm to 15 mm in only 24 days, whereas Imaizumi et al. (2002) report of an aneurysm that grew from about 4 mm to 10 mm in one year. Kamitani et al. (1999) study the growth rate of a large population of unruptured cerebral saccular aneurysms. They report growth rates ranging from 1% up to 120% of size increase per year. The aneurysms in this study had sizes in the range of 2.0 to 25 mm. Thus, the wide scatter in growth rate data makes a general estimation of t_{cl} less meaningful. However, it may still be possible to make an estimation for a specific aneurysm, and in this way be able to predict the future growth scenario of that particular lesion. For example, if the geometry of a detected aneurysm is known at two stages of its history with, say, a year between measurements, the proposed growth model could be applied to estimate the future growth of this aneurysm. This kind of prediction could actually help clinicians decide whether or not the aneurysm is or will become critical or not.

In summary, a new theoretical model for the growth of saccular cerebral aneurysms has been proposed. The continuous turnover of collagen is taken to be the driving mechanism in aneurysmal growth, and the collagen production depends on the

cyclic deformation of fibroblasts, that are taken to be spread throughout the tissue. The model is able to predict aneurysms with the berry-like shape often observed clinically, and the predicted wall stresses correlate well with the experimentally obtained ultimate stresses of this kind of tissue. The pre-stretch λ_{pre}, by which newly produced collagen is deposited, turns out to be of pivotal importance for growth stability and growth speed of the aneurysm.

Acknowledgments. Financial support for this research was partly provided by @neurIST, an Integrated EU Project (Call Identifier FP6-2004-IST-4). This support is gratefully acknowledged.

References

AAssar, O. S., Fujiwara, N. H., Marx, W. F., Matsumoto, A. H., Kallmes, D. F., 2003. Aneurysm growth, elastinolysis, and attempted doxycycline inhibition of elastase-induced aneurysms in rabbits. J. Vasc. Interv. Radiol. 14, 1427–1432.

Abdul-Hussien, H., Soekhoe, R. G., Weber, E., von der Thüsen, J. H., Kleemann, R., Mulder, A., van Bockel, J. H., Hanemaaijer, R., Lindeman, H. H., 2007. Collagen degradation in the abdominal aneurysm: a conspiracy of matrix metalloproteinase and cysteine collagenases. Am. J. Pathology 170, 809–817.

Abruzzo, T., Shengelaia, G. G., Dawson 3rd, R. C., Owens, D. S., Cawley, C. M., Gravanis, M. B., 1998. Histologic and morphologic comparison of experimental aneurysms with human intracranial aneurysms. Am. J. Neuroradiol. 19, 1309–1314.

Anidjar, S., Dobrin, P. B., Eichorst, M., Graham, G. P., Chejfec, G., 1992. Correlation of inflammatory infiltrate with the enlargement of experimental aortic aneurysms. J. Vasc. Surg. 16, 139–147.

Austin, G., Fisher, S., Dickson, D., Anderson, D., Richardson, S., 1993. The significance of the extracellular matrix in intracranial aneurysms. Ann. Clin. Lab. Sci. 23, 97–105.

Baek, S., Rajagopal, K. R., Humphrey, J. D., 2006. A theoretical model of enlarging intracranial fusiform aneurysms. J. Biomech. Eng. 128, 142–149.

Barocas, V. H., Moon, A. G., Tranquillo, R. T., 1995. The fibroblast–populated collagen microsphere assay of cell traction force – Part 2: Measurement of the cell traction parameter. J. Biomech. Eng. 117, 161–170.

Birk, D. E., Zycband, E. I., Winkelmann, D. A., Trelstad, R. L., 1990. Collagen fibrillogenesis in situ. Discontinuous segmental assembly in extracellular compartments. Ann. N.Y. Acad. Sci. 580, 176–194.

Brisman, J. L., Song, J. K., Newell, D. W., 2006. Cerebral aneurysms. N. Engl. J. Med. 355, 928–939.

Butt, R. P., Laurent, G. J., Bishop, J. E., 1995. Mechanical load and polypeptide growth factors stimulate cardiac fibroblast activity. Ann. N.Y. Acad. Sci. 752, 387–393.

Canham, P. B., Finlay, H. M., Dixon, J. G., Ferguson, S. E., 1991a. Layered collagen fabric of cerebral aneurysms quantitatively assessed by the universal stage and polarized light microscopy. Anat. Rec. 231, 579–592.

Canham, P. B., Finlay, H. M., Kiernan, J. A., Ferguson, G. G., 1999. Layered structure of saccular aneurysms assessed by collagen birefringence. Neurol. Res. 21, 618–626.

Canham, P. B., Finlay, H. M., Tong, S. Y., 1996. Stereological analysis of the layered collagen of human intracranial aneurysms. J. Microscopy 183, 170–180.

Canham, P. B., Korol, R. M., Finlay, H. M., Hammond, R. R., Holdsworth, D. W., Ferguson, G. G., Lucas, A. R., 2006. Collagen organization and biomechanics of the arteries and aneurysms of the human brain. In: Holzapfel, G. A., Ogden, R. W. (Eds.), Mechanics of Biological Tissue. Springer-Verlag, Heidelberg, pp. 307–322.

Canham, P. B., Talman, E. A., Finlay, H. M., Dixon, J. G., 1991b. Medial collagen organization in human arteries of the heart and brain by polarized light microscopy. Conn. Tiss. Res. 26, 121–134.

Canham, P. B., Whittaker, P., Barwick, S. E., Schwab, M. E., 1992. Effect of pressure on circumferential order of adventitial collagen in human brain arteries. Can. J. Physiol. Pharmacol. 70, 296–305.

Chatziprodromou, I., Tricoli, A., Poulikakos, D., Ventikos, Y., 2007. Haemodynamics and wall remodelling of a growing cerebral aneurysm: a computational model. J. Biomech. 40, 412–426.

Chen, P. R., Frerichs, K., Spetzler, R., 2004. Natural history and general management of unruptured intracranial aneurysms. Neurosurg. Focus 17, E1.

Cisneros, D. A., Hung, C., Franz, C. M., Muller, D. J., 2006. Observing growth steps of collagen self-assembly by time-lapse high-resolution atomic force microscopy. J. Struct. Biol. 154, 232–245.

Coulson, R. J., Cipolla, M. J., Vitullo, L., Chesler, N. C., 2004. Mechanical properties of rat middle cerebral arteries with and without myogenic tone. J. Biomech. Eng. 126, 76–81.

Cukierman, E., Pankov, R., Stevens, D. R., Yamada, K. M., 2001. Taking cell–matrix adhesions to the third dimension. Science 294, 1708–1712.

Dembo, M., Wang, Y. L., 1999. Stresses at the cell–to–substrate interface during locomotion of fibroblasts. Biophys. J. 76, 2307–2316.

Dobrin, P. B., Canfield, T. R., 1984. Elastase, collagenase, and the biaxial elastic properties of dog carotid artery. Am. J. Physiol. 247, H124–H131.

Eastwood, M., McGrouther, D. A., Brown, R. A., 1998. Fibroblast responses to mechanical forces. Proc. Inst. Mech. Eng. 212, 85–92.

Engler, A., Bacakova, L., Newman, C., Hategan, A., Griffin, M., Discher, D., 2004. Substrate compliance versus ligand density in cell on gel responses. Biophys. J. 86, 617–628.

Espinosa, F., Weir, B., Noseworthy, T., 1984. Rupture of an experimentally induced aneurysm in a primate. Can. J. Neurol. Sci. 11, 64–68.

Feigin, V. L., Rinkel, G. J. E., Lawes, C. M. M., Algra, A., Bennett, D. A., van Gijn, J., Anderson, C. S., 2005. Risk factors for subarachnoid hemorrhage. Stroke 36,

2773–2780.

Finlay, H. M., Dixon, J. G., Canham, P. B., 1991. Fabric organization of the subendothelium of the human brain artery by polarized-light microscopy. Arterioscler. Thromb. 11, 681–690.

Finlay, H. M., McCullough, L., Canham, P. B., 1995. Three-dimensional collagen organization of human brain arteries at different transmural pressures. J. Vasc. Res. 32, 301–312.

Finlay, H. M., Whittaker, P., Canham, P. B., 1998. Collagen organization in the branching region of human brain arteries. Stroke 29, 1595–1601.

Fried, I., 1982. Finite element computation of large rubber membrane deformations. Int. J. Numer. Meth. Eng. 18, 653–660.

Friedl, P., Bröcker, E.-B., 2000. The biology of cell locomotion within three-dimensional extracellular matrix. Cell Mol. Life Sci. 57, 42–64.

Friedrichs, J., Taubenberger, A., Franz, C. M., Muller, D. J., 2007. Cellular remodeling of individual collagen fibrils visualized by time–lapse AFM. J. Mol. Biol. 372, 594–607.

Grinnell, F., 2003. Fibroblast biology in three–dimensional collagen matrices. Trends in Cell Biology 13, 264–269.

Hashimoto, N., Handa, H., Nagata, I., Hazama, F., 1984. Animal model of cerebral aneurysms: pathology and pathogenesis of induced cerebral aneurysms in rats. Neurol. Res. 6, 33–40.

Hassler, O., 1972. Scanning electron microscopy of saccular intracranial aneurysms. Am. J. Pathology 68, 511–519.

Holzapfel, G. A., 2000. Nonlinear Solid Mechanics. A Continuum Approach for Engineering. John Wiley & Sons, Chichester.

Huang, D., Chang, T. R., Aggarwal, A., Lee, R. C., Ehrlich, H. P., 1993. Mechanisms and dynamics of mechanical strengthening in ligament-equivalent fibroblast-populated collagen matrices. Ann. Biomed. Eng. 21, 289–305.

Humphrey, J. D., 1999. Remodeling of a collagenous tissue at fixed lengths. J. Biomech. Eng. 121, 591–597.

Humphrey, J. D., 2001. Stress, strain and mechanotransduction in cells. J. Biomech. Eng. 123, 638–641.

Humphrey, J. D., 2002. Cardiovascular Solid Mechanics. Cells, Tissues, and Organs. Springer-Verlag, New York.

Humphrey, J. D., Rajagopal, K. R., 2002. A constrained mixture model for growth and remodeling of soft tissues. Math. Model. Meth. Appl. Sci. 12, 407–430.

Imaizumi, S., Onuma, T., Motohashi, O., Kameyama, M., 2002. Growth of small unruptured intracranial aneurysm. Surg. Neurol. 58, 155–157.

Jamous, M. A., Nagahiro, S., Kitazato, K. T., Satoh, K., Satomi, J., 2005. Vascular corrosion cases mirroring early morphological changes that lead to the formation of saccular cerebral aneurysm: an experimental study in rats. J. Neurosurg. 102, 532–535.

Jiang, H., Grinnell, F., 2005. Cell–matrix entanglement and mechanical anchorage of fibroblasts in three–dimensional collagen matrices. Mol. Biol. Cell 16, 5070–5076.

Kamitani, H., Masuzawa, H., Kanazawa, I., Kubo, T., 1999. Bleeding risk in unruptured and residual cerebral aneurysms – angiographic annual growth rate in nineteen patients. Acta Neurochir. (Wien) 141, 153–159.

Kamphorst, W., Yong-Zhong, G., van Alphen, A. M., 1991. Pathological changes in experimental saccular aneurysms in the carotid artery of the rat. Neurol. Res. 13, 55–59.

Kim, C., Cervos-Navarro, J., 1991. Spontaneous saccular cerebral aneurysm in a rat. Acta Neurochir. (Wien) 109, 63–65.

Kim, C., Cervos-Navarro, J., Kikuchi, H., Hashimoto, N., Hazama, F., 1992. Alterations in cerebral vessels in experimental animals and their possible relationship to the development of aneurysms. Surg. Neurol. 38, 331–337.

Kojima, M., Handa, H., Hashimota, N., Kim, C., Hazama, F., 1986. Early changes of experimentally induced cerebral aneurysms in rats: scanning electron microscopic study. Stroke 17, 835–841.

Kondo, S., Hashimoto, N., Kikuchi, H., Hazama, F., Nagata, I., Kataoka, H., Rosenblum, W. I., 1998. Apoptosis of medial smooth muscle cells in the development of saccular cerebral aneurysms in rats. Stroke 29, 181–189.

Kroon, M., Holzapfel, G. A., 2007a. A model for saccular cerebral aneurysm growth by collagen fibre remodelling. J. Theor. Biol. 247, 775–787.

Kroon, M., Holzapfel, G. A., 2007b. Modelling of saccular aneurysm growth in a human middle cerebral artery. J. Biomech. Eng.In press.

Kyriacou, S. K., Schwab, C., Humphrey, J. D., 1996. Finite element analysis of nonlinear orthotropic hyperelastic membranes. Comput. Mech. 18, 269–278.

Lee, C.-Y., Liu, X., Smith, C. L., Zhang, X., Hsu, H.-C., Wang, D.-Y., Luo, Z.-P., 2004. The combined regulation of estrogen and cyclic tension on fibroblast synthesis derived from anterior cruciate ligament. Matrix Biol. 23, 323–329.

Lin, H., Clegg, D. O., Lal, R., 1999. Imaging real–time proteolysis of single collagen I molecules with an atomic force microscope. Biomechistry 38, 9956–9963.

Lo, C.-M., Wang, H.-B., Dembo, M., Wang, Y., 2000. Cell movement is guided by the rigidity of the substrate. Biophys. J. 79, 144–152.

MacDonald, D. J., Finlay, H. M., Canham, P. B., 2000. Directional wall strength in saccular brain aneurysms from polarized light microscopy. Ann. Biomed. Eng. 28, 533–542.

Majamaa, K., Savolainen, E. R., Myllylä, V. V., 1992. Synthesis of structurally unstable type III procollagen in patients with cerebral artery aneurysm. Biochim. Biophys. Acta 1138, 191–196.

Matsubara, S., Hadeishi, H., Suzuki, A., Yasui, N., Nishimura, H., 2004. Incidence and risk factors for the growth of unruptured cerebral aneurysms: observation using serial computerized tomography angiography. J. Neurosurg. 101, 908–914.

McMillan, W. D., Patterson, B. K., Keen, R. R., Pearce, W. H., 1995. In situ localization and quantification of seventy-two-kilodalton type IV collagenase in aneurysmal, occlusive, and normal aorta. J. Vasc. Surg. 22, 295–305.

Meshel, A. S., Wei, Q., Adelstein, R. S., Sheetz, M. P., 2005. Basic mechanism of three–dimensional collagen fibre transport by fibroblasts. Nature Cell Biol. 7, 157–164.

Mettinger, K. L., 1982. Fibromuscular dysplasia and the brain. II. Current concept of the disease. Stroke 13, 53–58.

Mimata, C., Kitaoka, M., Nagahiro, S., Iyama, K., Hori, H., Yoshioka, H., Ushio, Y., 1997. Differential distribution and expressions of collagens in the cerebral aneurysmal wall. Acta Neuropath. (Berlin) 94, 197–206.

Miskolczi, L., Guterman, L. R., Flaherty, J. D., Hopkins, L. N., 1998. Saccular aneurysm induction by elastase digestion of the arterial wall: a new animal model. Neurosurgery 43, 595–601.

Monson, K. L., Goldsmith, W., Barbaro, N. M., Manley, G. T., 2003. Axial mechanical properties of fresh human cerebral blood vessels. J. Biomech. Eng. 125, 288–294.

Monson, K. L., Goldsmith, W., Barbaro, N. M., Manley, G. T., 2005. Significance of source and size in the mechanical response of human cerebral blood vessels. J. Biomech. 38, 737–744.

Murphy, G., Reynolds, J., 1985. Current views of collagen degradation. Bioessays 2, 55–60.

Pelham, R. J., Wang, Y., 1997. Cell locomotion and focal adhesions are regulated by substrate flexibility. Proc. Natl. Acad. Sci. USA 94, 13661–13665.

Pentimalli, L., Modesti, A., Vignati, A., Marchese, E., Albanese, A., Di Rocco, F., Coletti, A., Di Nardo, P., Fantini, C., Tirpakova, B., Maira, G., 2004. Role of apoptosis in intracranial aneurysm rupture. J. Neurosurg. 101, 1018–1025.

Poole, K., Khairy, K., Friedrichs, J., Franz, C., Cisneros, D. A., Howards, J., Mueller, D., 2005. Molecular–scale topographic cues induce the orientation and directional movement of fibroblasts on two–dimensional collagen surfaces. J. Mol. Biol. 349, 380–386.

Rachev, A., Stergiopulos, N., Meister, J.-J., 1996. Theoretical study of dynamics of arterial wall remodeling in response to changes in blood pressure. J. Biomech. 29, 635–642.

Rinkel, G. J. E., Djibuti, M., Algra, A., van Gijn, J., 1998. Prevalence and risk of rupture of intracranial aneurysms. Stroke 29, 251–256.

Rowe, A. J., Finlay, H. M., Canham, P. B., 2003. Collagen biomechanics in cerebral arteries and bifurcations assessed by polarizing microscopy. J. Vasc. Res. 40, 406–415.

Ryan, J. M., Humphrey, J. D., 1999. Finite element based predictions of preferred material symmetries in saccular aneurysms. Ann. Biomed. Eng. 27, 641–647.

Sakaki, T., Kohmura, E., Kishiguchi, T., Yuguchi, T., Yamashita, T., Hayakawa, T., 1997. Loss and apoptosis of smooth muscle cells in intracranial aneurysms. Studies with in situ DNA end labeling and antibody against single-stranded DNA. Acta Neurochir. 139, 469–474.

Scanarini, M., Mingrino, S., Giordano, R., Baroni, A., 1978. Histological and ultrastructural study of intracranial saccular aneurysmal wall. Acta Neurochir. (Wien) 43, 171–182.

Schievink, W. I., 1997. Intracranial aneurysms. N. Engl. J. Med. 336, 28–40.

Scott, S., Ferguson, G. G., Roach, M. R., 1972. Comparison of the elastic properties of human intracranial arteries and aneurysms. Can. J. Physiol. Pharmacol. 50,

328–332.

Sluijter, J. P. G., Smeets, M. B., Velema, E., Pasterkamp, G., de Kleijn, D. P. V., 2004. Increased collagen turnover is only partly associated with collagen fiber deposition in the arterial response to injury. Cardiovasc. Res. 61, 186–195.

Smith, J. F. H., Canham, P. B., Starkey, J., 1981. Orientation of collagen in the tunica adventitia of the human cerebral artery measured with polarized light and the universal stage. J. Ultrastruct. Res. 77, 133–145.

Stehbens, W. E., 1963. Ultrastructure of aneurysms. Arch. Neurol. 32, 798–807.

Steiger, H. J., 1990. Pathophysiology of Development and Rupture of Cerebral Aneurysms (Acta Neurochirurgica Supplementum 48). Springer-Verlag, Wien.

Suzuki, J., Ohara, H., 1978. Clinicopathological study of cerebral aneurysms. Origin, rupture, repair and growth. J. Neurosurg. 48, 505–514.

Taber, L. A., Humphrey, J. D., 2001. Stress-modulated growth, residual stress, and vascular heterogeneity. J. Biomech. Eng. 123, 528–535.

Tóth, B. K., Raffai, G., Bojtár, I., 2005. Analysis of mechanical parameters of human brain aneurysm. Acta of Bioeng. and Biomech. 7, 4–22.

Tóth, M., Násady, G. L., Nyáry, I., Kerényi, T., Orosz, M., Molnárka, G., Monos, E., 1998. Sterically inhomogenous viscoelastic behavior of human saccular cerebral aneurysms. J. Vasc. Res. 35, 345–355.

Walmsley, J. G., Campling, M. R., Chertkow, H. M., 1983. Interrelationships among wall structure, smooth muscle orientation, and contraction in human major cerebral arteries. Stroke 14, 781–790.

Watton, P. N., Hill, N. A., Heil, M., 2004. A mathematical model for the growth of the abdominal aortic aneurysm. Biomech. Model. Mechanobio. 3, 98–113.

Webster, M. W., McAuley, C. E., Steed, D. L., Miller, D. D., Evans, C. H., 1991. Collagen stability and collagenolytic activity in the normal and aneurysmal human abdominal aorta. Am. J. Surg. 161, 635–638.

Wermer, M. J. H., van der Schaaf, I. C., Velthuis, B. K., Algra, A., Buskens, E., Rinkel, G. J. E., 2005. Follow–up screening after subarachnoid haemorrhage: frequency and determinants of new aneurysms and enlargement of existing aneurysms. Brain 128, 2421–2429.

Weyts, F. A. A., Bosmans, B., Niesing, R., Leeuwen, J. P. T. M., Weinans, H., 2003. Mechanical control of human osteoblast apoptosis and proliferation in relation to differentiation. Calcif. Tissue Int. 72, 505–512.

Whittaker, P., Schwab, M. E., Canham, P. B., 1988. The molecular organization of collagen in saccular aneurysms assessed by polarized light microscopy. Conn. Tiss. Res. 17, 43–54.

Wiebers, D. O., Whisnant, J. P., O'Fallon, W. M., 1981. The natural history of unruptured intracranial aneurysms. N. Engl. J. Med. 304, 696–698.

Wille, J. J., Elson, E. L., Okamoto, R. J., 2006. Cellular and matrix mechanics of bioartificial tissues during continuous cyclic stretch. Ann. Biomed. Eng. 34, 1678–1690.

Wu, Q.-Q., Chen, Q., 2000. Mechanoregulation of chondrocyte proliferation, maturation, and hypertrophy: ion-channel dependent transduction of matrix deformation signals. Exp. Cell Res. 256, 383–391.

Yamaki, T., Yoshino, E., Higuchi, T., 1986. Rapidly growing aneurysm. Surg. Neurol. 26, 301–305.

Zhang, D., Zhao, J., Sun, Y., Wang, S., Tai, W. H., Cochrane, D. D., Li, J., 2003. Pathological observation of brain arteries and spontaneous aneurysms in hypertensive rats. Chin. Med. J. (Engl). 116, 424–427.